

Bachelor Assignment
Computational Material Sciences

-

Interface Models for Spin Transport through
Magnetic Multilayers

Author: Bas Schuttrups

May 2015

Contents

1	Introduction	3
2	Theory	5
2.1	Valet-Fert	5
2.1.1	Change of variables	6
2.2	Transfer Matrices	7
2.3	Interface Models	8
2.3.1	Valet-Fert	9
2.3.2	Bass-Pratt	9
2.3.3	6 Resistances	10
3	Implementation	13
3.1	Multiply layer & interface transfer matrices	13
3.2	Set up the linear system	14
3.3	Calculate boundary values	15
3.4	Calculate integration constants	16
3.5	Precision	17
4	Results	19
4.1	Identity Interface Model	19
4.1.1	NFN	19
4.1.2	Spin Valves	21
4.2	Non-identity Interface Models	22
4.3	Interface Parameter Dependent Step Sizes	24
4.3.1	Valet-Fert	24
4.3.2	Bass-Pratt	27
4.3.3	6 Resistances	29
5	Conclusions	31
6	Future Recommendations	33
	References	35

Chapter 1

Introduction

Giant magnetoresistance (GMR) refers to an effect that occurs in thin film structures, composed of alternating ferromagnetic and nonmagnetic layers with thicknesses comparable to the spin-diffusion length. If an electric current is passed through such a structure perpendicular to the layers (which makes it a current-perpendicular-to-the-plane, or CPP-MR geometry), the total electrical resistance depends on the alignment of the magnetizations of adjacent layers.

If we now create a so called 'spin valve': one layer with a magnetic field independent magnetization and one with a field dependent magnetization, we have created a magnetic field sensor, which is the main application of CPP-MR structures. Magnetic field sensors are then used in hard disk drive read heads, for example.

In 1993, Thierry Valet and Albert Fert (VF) published a paper in which they found general solutions for the spin-dependent chemical potentials and current densities in these ferro- and nonmagnetic layers. This has been done before, but VF were the first to do it without assuming that the layer thickness is much larger than the spin-diffusion length. Therefore, their results allow for a more accurate calculation of the spin accumulation in CPP-MR structures and thereby GMR.

This report is about the implementation of a solver, which takes these general solutions from the VF paper, uses a transfer matrix method to find the system specific boundary values and thereby obtain a solution to the CPP-MR system. To simulate the behaviour upon transport through the interfaces between the layers, three different interface models were implemented. The results of this solver are analyzed and discussed, with an emphasis on the comparison between the different interface models.

Chapter 2

Theory

2.1 Valet-Fert

The paper by VF¹ uses a macroscopic approach to solving these CPP-MR geometries for the spin-dependent chemical potential and current density through the linearized Boltzmann Equation (LBE). It also shows that this approach is justified for any layer thickness for the limit where the spin-diffusion length (SDL, l_{sf}) is much longer than the mean free path (MFP, λ_{sf}). We can safely make this assumption, because the ratio of the SDL and MFP depends on the strength of the spin orbit coupling in a material, which is usually weak, meaning that spin-flip scattering occurs far less frequently than momentum scattering, i.e. $SDL \gg MFP$.

The Boltzmann equation is a macroscopic equation that describes the statistical behavior of, in our case, the charge carrier density inside a metal or semiconductor. Its principle statement for a steady state is as follows:

$$\left. \frac{\partial f_s}{\partial t} \right]_{\text{diffusion}} + \left. \frac{\partial f_s}{\partial t} \right]_{\text{field}} + \left. \frac{\partial f_s}{\partial t} \right]_{\text{scattering}} = 0 \quad (2.1)$$

with $f_s(z, \mathbf{v})$ the charge carrier distribution function with spin s and velocity \mathbf{v} at position z .

The LBE is obtained by filling in the three terms in 2.1 and dropping all the terms of order E^2 and higher. VF¹ states the LBE as follows:

$$\underbrace{v_z \frac{\partial f_s}{\partial z}(z, \mathbf{v})}_{\text{diffusion}} - \underbrace{eE(z)v_z \frac{\partial f^0}{\partial \epsilon}(v)}_{\text{field}} = \underbrace{\int d^3v' \delta[\epsilon(v') - \epsilon(v)] P_s[z, \epsilon(v)] [f_s(z, \mathbf{v}') - f_s(z, \mathbf{v})]}_{\text{scattering}} + \int d^3v' \delta[\epsilon(v') - \epsilon(v)] P_{sf}[z, \epsilon(v)] [f_{-s}(z, \mathbf{v}') - f_s(z, \mathbf{v})] \quad (2.2)$$

with $\epsilon(v) = \frac{1}{2}mv^2$ the electron energy, $E(z)$ the local electric field and P_s and P_{sf} respectively the spin conserving and spin-flipping transition probabilities. The two

integrals on the right-hand side represent the summation over respectively all spin conserving and spin-flipping scatterings.

The distribution function is then written down by adding up the equilibrium density (the Fermi-Dirac distribution) and a term for small perturbations:

$$f_s(z, \mathbf{v}) = f^0(v) + \frac{\partial f^0}{\partial \epsilon} \left\{ \left[\mu^0 - \mu_s(z) \right] + g_s(z, \mathbf{v}) \right\} \quad (2.3)$$

with μ^0 the equilibrium chemical potential, f^0 the Fermi-Dirac distribution, $(\partial f^0 / \partial \epsilon) g_s$ the anisotropic part of the perturbation and $(\partial f^0 / \partial \epsilon) [\mu^0 - \mu_s]$ the isotropic perturbation due to spin-dependent local variations in the chemical potential, caused by spin accumulation. Here, $\mu_s(z) (= \mu^\pm(z))$ is the spin-dependent chemical potential as a function of position.

Using 2.3, one can derive the following macroscopic transport equations from the LBE, which are valid in the limit $\lambda_{sf}/l_{sf} \ll 1$:

$$\frac{e}{\sigma_s} \frac{\partial J_s}{\partial z} = \frac{\mu_s - \mu_{-s}}{l_s^2}, \quad (2.4a)$$

$$J_s = \frac{\sigma_s}{e} \frac{\partial \mu_s}{\partial z} \quad (2.4b)$$

where $J_s (= J^\pm)$, σ_s and l_s are the spin-dependent current density, conductivity and SDL respectively. These two equations can be rewritten to a spin-diffusion type equation, namely:

$$\frac{\partial^2 \Delta \mu}{\partial z^2} = \frac{\Delta \mu}{l_{sf}^2} \quad (2.5)$$

with $\Delta \mu \equiv \frac{1}{2}(\mu^+ - \mu^-)$. VF then solve 2.5 and obtain the following general solutions:

$$\mu_n^\pm(z) = \alpha_n J z + K_1^{(n)} \pm (1 \pm \beta_n) \left[K_2^{(n)} e^{z/l_{sf}^{(n)}} + K_3^{(n)} e^{-z/l_{sf}^{(n)}} \right] \quad (2.6a)$$

$$J_n^\pm(z) = (1 \mp \beta_n) \frac{J}{2} \pm \frac{1}{r_{sf}^{(n)}} \left[K_2^{(n)} e^{z/l_{sf}^{(n)}} - K_3^{(n)} e^{-z/l_{sf}^{(n)}} \right] \quad (2.6b)$$

with $\alpha_n \equiv (1 - \beta_n^2) e \rho_n^*$, $r_{sf}^{(n)} \equiv e \rho_n^* l_{sf}^{(n)}$, where β_n is the magnetization, α_n the electrical resistivity of the layer and e the elementary charge. $K_{1,2,3}^{(n)}$ are integration constants and n denotes the layer index. Therefore, all the material-specific variables are n-dependent.

2.1.1 Change of variables

In this report, two different sets of variables are used. The first one is the set used in the paper by VF and is denoted with a tilde:

$$\tilde{\mathbf{x}} = \begin{pmatrix} \mu^+ \\ \mu^- \\ J^+ \\ J^- \end{pmatrix}. \quad (2.7)$$

The second set is defined as in 2.8 and is denoted without a tilde. These are the variables we will be working with. We also define a matrix $\mathbf{\Gamma}$, which transforms the set used by VF into the new set:

$$\mathbf{x} = \begin{pmatrix} \mu \\ \Delta\mu \\ \Delta J \\ J \end{pmatrix} \equiv \begin{pmatrix} \frac{1}{2}(\mu^+ + \mu^-) \\ \frac{1}{2}(\mu^+ - \mu^-) \\ J^+ - J^- \\ J^+ + J^- \end{pmatrix} = \begin{pmatrix} \frac{1}{2} & \frac{1}{2} & 0 & 0 \\ \frac{1}{2} & -\frac{1}{2} & 0 & 0 \\ 0 & 0 & 1 & -1 \\ 0 & 0 & 1 & 1 \end{pmatrix} \tilde{\mathbf{x}} \equiv \mathbf{\Gamma} \tilde{\mathbf{x}} \quad (2.8)$$

so that the solutions from VF become:

$$\mu^{(n)}(z) = \alpha_n J z + K_1^{(n)} + \beta_n \Delta\mu^{(n)}(z) \quad (2.9a)$$

$$\Delta\mu^{(n)}(z) = K_2^{(n)} e^{z/l_{\text{sf}}^{(n)}} + K_3^{(n)} e^{-z/l_{\text{sf}}^{(n)}} \quad (2.9b)$$

$$\Delta J^{(n)}(z) = -\beta_n J + \frac{1}{r_{\text{sf}}^{(n)}} \left[K_2^{(n)} e^{z/l_{\text{sf}}^{(n)}} - K_3^{(n)} e^{-z/l_{\text{sf}}^{(n)}} \right] \quad (2.9c)$$

$$J^{(n)}(z) = J. \quad (2.9d)$$

Note that $\mu = qV = -eV$ has the same properties as any potential and can be chosen relative to any arbitrary reference value (i.e. ground). Mathematically, this is done through the coefficient $K_1^{(n)}$. Also note that the current density J is a constant since the system is in a steady state and current is conserved.

Secondly, since we are dealing with a steady-state system of a series of layers, the total current density J has to be constant throughout the system.

2.2 Transfer Matrices

Often the transport equations 2.4 are numerically integrated to simulate the behavior of magnetic multilayer systems. One could pose this is a bit redundant for we already possess the general solutions to the system (2.6). In this report, a possibly smarter and faster method using transfer matrices is developed and implemented.

Since the general solutions to the system are already known, the goal of our method is to provide a way to calculate the unknowns in these general solutions (i.e. integration constants).

In order to do this, our method makes use of the fact that we are working in the linear response regime, i.e. that the variables in the system only depend linearly on each other. This means that the state vector, containing those variables on one side of the system or any component of the system can be expressed as a linear function of the state vector elements on the other side of that system, which can be written down as a matrix product:

$$\mathbf{x}_2 = \mathbf{W}_{21} \mathbf{x}_1 \quad (2.10)$$

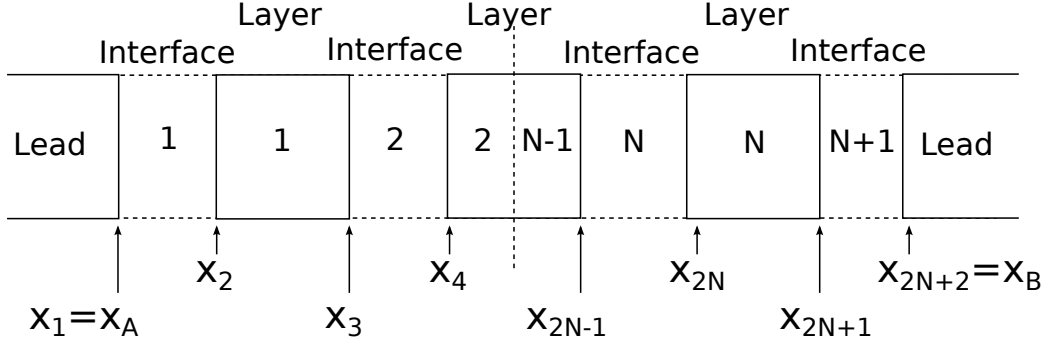


Figure 2.1: Schematic representation of the used system.

where the matrix \mathbf{W}_{21} is called the transfer matrix and \mathbf{x}_i is the state vector at some point, indicated by the subscript i , between two components and therefore contains the boundary values at that point (see figure 2.1).

So we need an expression for the transfer matrix of each layer, and for the transfer matrix of each interface. In the next section we will consider models for interfaces. Here we state the result for a layer that we derived from 2.6:

$$\mathbf{W}_{\text{layer}}^{\text{VF}} = \begin{pmatrix} 1 & \beta (\cosh \delta - 1) & \beta r_{\text{sf}} \sinh \delta & (1 - \beta^2) r_{\text{sf}} \delta + \beta^2 r_{\text{sf}} \sinh \delta \\ 0 & \cosh \delta & r_{\text{sf}} \sinh \delta & \beta r_{\text{sf}} \sinh \delta \\ 0 & \frac{1}{r_{\text{sf}}} \sinh \delta & \cosh \delta & \beta (\cosh \delta - 1) \\ 0 & 0 & 0 & 1 \end{pmatrix} \quad (2.11)$$

where $\delta \equiv t/l_{\text{sf}}$, with t the layer thickness. For nonmagnetic layers $\beta = 0$ so the transfer matrix becomes quite simple.

Note the simple form of the first column and the bottom row. This is no coincidence: Because the reference for the electrochemical potential is arbitrary and constant, only μ_2 can depend on μ_1 and the other variables cannot depend on μ_1 . Hence the form of the first column.

Also, J is constant throughout the system. Hence the form of the bottom row. Finally, note that the contents of the matrix only depend on three constants: β , δ and $r_{\text{sf}} = e\rho^*l_{\text{sf}}^{(n)}$.

2.3 Interface Models

Determining how the interfaces between the layers affect the variables is less straight-forward. In this report, we take a look at three different models which can be used to derive a transfer matrix for the interfaces. The first two of these interface models are taken from literature, the third one is an original model.

2.3.1 Valet-Fert

The first interface model is the model used in the paper by VF. This model, also known as the two-current series resistor (2CSR) model, basically replaces the interface by a circuit-diagram which can be seen in figure 2.2.

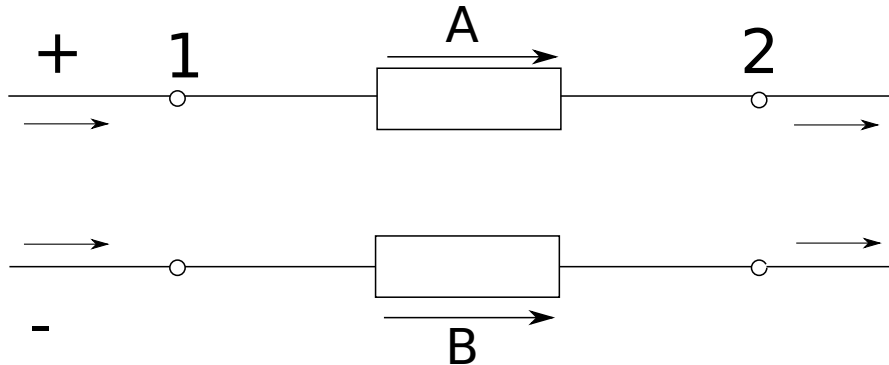


Figure 2.2: Circuit diagram containing two series resistors used in the VF interface model.

The transfer matrix for the VF model looks as follows:

$$\mathbf{W}_{\text{int}}^{\text{VF}} = \begin{pmatrix} 1 & 0 & \frac{1}{4}(R_A - R_B) & \frac{1}{4}(R_A + R_B) \\ 0 & 1 & \frac{1}{4}(R_A + R_B) & \frac{1}{4}(R_A - R_B) \\ 0 & 0 & 1 & 0 \\ 0 & 0 & 0 & 1 \end{pmatrix} \quad (2.12)$$

with R_A and R_B the resistances for the up and the down spin current respectively.

The 2CSR model assumes no spin-flipping occurs at the interfaces. This can be seen in the circuit diagram (figure 2.2) by the absence of connections between the spin up and spin down nodes. This means that the spin-dependent currents flow through the interfaces as if they are flowing through a system of two independent, parallel series connections, meaning that the spin-dependent currents remain constant (i.e. $J_2^\pm = J_1^\pm$).

In other words, the VF interface model describes two channel interface transport using two independent parameters (R_A and R_B).

2.3.2 Bass-Pratt

The second interface model is a model introduced by W.P. Pratt and J. Bass³. They model the behavior of an interface by replacing it by a virtual layer. Mathematically, this means using the VF layer transfer matrix as the interface transfer matrix from 2.11. However, we rewrite the elements such that $\gamma = \beta, r \equiv e\rho^*t(1 - \gamma^2) =$

$r_{\text{sf}}\delta(1 - \gamma^2)$, and δ . This definition makes r the interface resistance. These changes lead to the Bass-Pratt interface transfer matrix:

$$\mathbf{W}_{\text{int}}^{\text{BP}} = \begin{pmatrix} 1 & \gamma (\cosh \delta - 1) & \frac{\gamma r}{\delta(1-\gamma^2)} \sinh \delta & r + \frac{\gamma^2 r}{\delta(1-\gamma^2)} \sinh \delta \\ 0 & \cosh \delta & \frac{r}{\delta(1-\gamma^2)} \sinh \delta & \frac{\gamma r}{\delta(1-\gamma^2)} \sinh \delta \\ 0 & \frac{\delta(1-\gamma^2)}{r} \sinh \delta & \cosh \delta & \gamma (\cosh \delta - 1) \\ 0 & 0 & 0 & 1 \end{pmatrix}. \quad (2.13)$$

This means that the BP interface model describes interface transport three independent parameters.

2.3.3 6 Resistances

The third and final interface model is a new model, created by R. Wesselink². Just like the VF model, this model behaves as if the interfaces were replaced by an electrical circuit. However, this time the circuit contains not two but six resistances (see figure 2.3). Therefore, we call this model the 6 resistances (R6) model.

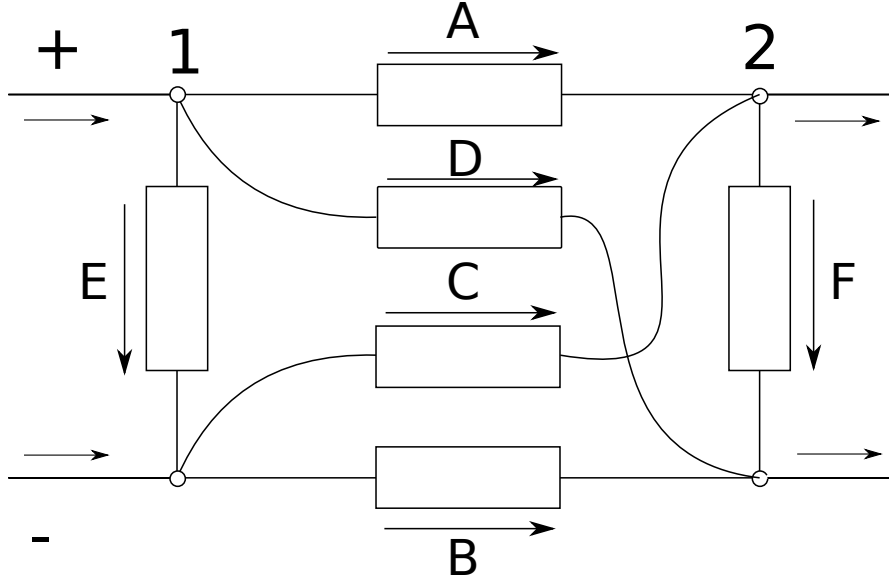


Figure 2.3: Circuit diagram containing six resistors, used in the R6 interface model.

By using a modified version of Ohm's law:

$$V_{\text{diff.}} = r \cdot I, \quad r > 0, \quad \mu = -eV, \quad J = I/A, \quad (2.14a)$$

$$\Rightarrow \mu_{\text{diff.}} = R_i \cdot J, \quad R_i > 0 \quad (2.14b)$$

it is possible to write down explicit expressions for the spin-dependent variables on side 2 in terms of the variables on side 1. Since these expressions are all linear, they yield the R6 interface transfer matrix:

$$\tilde{\mathbf{W}}_{\text{int}}^{\text{R6}} = \begin{pmatrix} \xi_{1++} & -\xi_{1+-} & R_{++} & -R_{+-} \\ -\xi_{1-+} & \xi_{1--} & -R_{-+} & R_{--} \\ Q & -Q & \xi_{2++} & -\xi_{2+-} \\ -Q & Q & -\xi_{2-+} & \xi_{2--} \end{pmatrix} \quad (2.15)$$

with:

$$\mathbf{G} = \begin{pmatrix} G_{++} & G_{+-} \\ G_{-+} & G_{--} \end{pmatrix} \equiv \begin{pmatrix} A & D \\ C & B \end{pmatrix}, \quad G_1^r \equiv E, \quad G_2^r \equiv F \quad (2.16a)$$

$$L_{1s} \equiv G_{ss} + G_{-s,s} + G_1^r, \quad L_{2s} \equiv G_{ss} + G_{s,-s} + G_2^r \quad (2.16b)$$

$$\xi_{1st} \equiv \frac{1}{\det \mathbf{G}} (G_{-s,-t} L_{1t} + G_{-s,t} G_1^r) \quad (2.16c)$$

$$\xi_{2st} \equiv \frac{1}{\det \mathbf{G}} (G_{-s,-t} L_{2s} + G_{s,-t} G_1^r) \quad (2.16d)$$

$$Q \equiv \frac{1}{4} \sum_{st} \left[\xi_{1st} \xi_{2st} \frac{\det \mathbf{G}}{G_{-s,-t}} + st \left(\frac{G_1^r G_2^r}{G_{st}} - G_{st} \right) \right] \quad (2.16e)$$

$$R_{st} \equiv \frac{1}{\det \mathbf{G}} G_{-s,-t}. \quad (2.16f)$$

Here, the definitions $A \equiv R_A^{-1}, B \equiv R_B^{-1}, \dots$ were used.

In this model the six parameters can be intuitively related to six different scattering processes:

1. A is related to the part of the incoming up-spin current that flows through the interface without spin-flipping.
2. B is related to the part of the incoming down-spin current that flows through the interface without spin-flipping.
3. C is related to the part of the incoming down-spin current that flows through the interface and ends up in a spin-flipped state.
4. D is related to the part of the incoming up-spin current that flows through the interface and ends up in a spin-flipped state
5. E is related to the part of the incident current from the left that undergoes a spin-flip and is reflected.
6. F is related to the part of the incident current from the right that undergoes a spin-flip and is reflected.

Chapter 3

Implementation

So the solver treated in this report takes the general solutions from VF¹ (2.6) and calculates the system-specific integration constants using transfer matrices and three different models for the interface transfer matrices. In order to do this, the solver performs four consecutive tasks:

First, the solver multiplies all layer and interface transfer matrices to obtain a transfer matrix for the entire system. After that, the solver takes the matrix expression for the entire system, which is an underdetermined linear system, and transforms it into a solvable one. The third step consists of solving this linear system and obtain the system boundary values. Finally, the solver uses these boundary values to calculate the integration constants for all the layers and with that obtain a solution to the system.

3.1 Multiply layer & interface transfer matrices

The first step the solver performs is calculating the elements of all the layer and interface transfer matrices. Once all the transfer matrices are known, they are all multiplied to obtain a single transfer matrix that describes the entire system:

$$\mathbf{x}_B = \begin{pmatrix} \mu \\ \Delta\mu \\ \Delta J \\ J \end{pmatrix}_B = \mathbf{W} \begin{pmatrix} \mu \\ \Delta\mu \\ \Delta J \\ J \end{pmatrix}_A = \mathbf{W} \mathbf{x}_A \quad (3.1)$$

where \mathbf{x}_A is the state vector on the far left side of the system and \mathbf{x}_B the state vector on the far right side of the system (see figure 2.1). This procedure can be mathematically described by:

$$\mathbf{W} = \mathbf{W}_{\text{int}}^{(N+1)} \prod_{i=1}^N \left[\mathbf{W}_{\text{layer}}^{(N+1-i)} \mathbf{W}_{\text{int}}^{(N+1-i)} \right] \quad (3.2)$$

where the superscripts denote the layer or interface number. The exact forms of the interface matrices depend on the interface model that is being used. Note that every system consists of N layers and $N + 1$ interfaces.

Furthermore, the system is nondimensionalized by dividing our set of variables $(\mu, \Delta\mu, \Delta J, J)$ by the scaling quantities respectively $(e, e, 1, 1)$. These scaling quantities were chosen according to the relationship

$-e \cdot V_{\text{diff.}} = \mu_{\text{diff.}} = -e \cdot r \cdot I$ and are therefore taking care of the order of magnitude difference between μ and J , which might become a problem computationally wise when calculating number in terms of both μ and J on a computer with a finite precision.

3.2 Set up the linear system

The second step consists of setting up a solvable, linear system of equations for the entire system and solving it.

The linear system is obtained by taking 3.1. However, this is an underdetermined system, consisting of four equations (four matrix rows) and eight unknowns $(\mu_A, \mu_B, \Delta\mu_A, \Delta\mu_B, \Delta J_A, \Delta J_B, J_A$ and $J_B)$ and is therefore not (yet) solvable.

To make it solvable, we need to make the number of unknowns equal to the number of equations. To do this, we start with the total current density J , which is constant throughout the system:

$$J_A = J_B = J. \quad (3.3)$$

This leaves us with a system containing six unknowns and three equations. Then, we make use of the fact that μ can be defined to be relative to any reference value or ground (as long as we are consistent about it). If we define μ_A as our ground:

$$\mu_A \equiv 0 \quad (3.4)$$

we have eliminated one unknown. This leaves us with a system of five unknowns and three equations.

Finally, we take a look at the general solutions from VF (2.6) and notice that both $\Delta\mu$ and ΔJ contain the same two exponential functions: $e^{+z/l_{sf}^{(n)}}$ and $e^{-z/l_{sf}^{(n)}}$. Since the leads are semi-infinite, the former would blow up in the right lead and the latter would blow up in the left lead. Because we know that $\Delta\mu$ and ΔJ go to zero over distance instead of blowing up, we know that this behavior is physically incorrect and thus that these exponential terms cannot exist. Mathematically, this means that the integration constants $K_2^{(A)}$ and $K_3^{(B)}$ are zero. Therefore, we can

now write for the left lead:

$$\Delta\mu^{(A)}(z) = K_2^{(A)} e^{+z/l_{sf}^{(A)}} \quad \Rightarrow \Delta\mu_A \equiv \Delta\mu^{(A)}(0) = K_2^{(A)} \quad (3.5a)$$

$$\Delta J^{(A)}(z) = \frac{1}{r_A} K_2^{(A)} e^{+z/l_{sf}^{(A)}} \quad \Rightarrow \Delta J_A \equiv \Delta J^{(A)}(0) = \frac{1}{r_A} K_2^{(A)} \quad (3.5b)$$

$$\Rightarrow \boxed{\Delta J_A = \frac{1}{r_A} \Delta\mu_A} \quad (3.5c)$$

and for the right lead:

$$\Delta\mu^{(B)}(z) = K_3^{(B)} e^{-z/l_{sf}^{(B)}} \quad \Rightarrow \Delta\mu_B \equiv \Delta\mu^{(B)}(0) = K_3^{(B)} \quad (3.6a)$$

$$\Delta J^{(B)}(z) = -\frac{1}{r_B} K_3^{(B)} e^{-z/l_{sf}^{(B)}} \quad \Rightarrow \Delta J_B \equiv \Delta J^{(B)}(0) = -\frac{1}{r_B} K_3^{(B)} \quad (3.6b)$$

$$\Rightarrow \boxed{\Delta J_B = -\frac{1}{r_B} \Delta\mu_B}. \quad (3.6c)$$

As can be seen in 3.5c and 3.6c, we have now obtained explicit expressions for ΔJ_A and ΔJ_B . If we now substitute these expressions back in our linear system of equations, we have effectively eliminated ΔJ_A and ΔJ_B from our set of unknowns, leaving us with a system of three equations and three unknowns ($\mu_B, \Delta\mu_A$ and $\Delta\mu_B$), which is no longer underdetermined and therefore solvable.

Rewriting the system into the form $\mathbf{M} \mathbf{x} = \mathbf{b}$ yields the following linear system:

$$\begin{pmatrix} w_{12} + \frac{w_{13}}{r_A} & 0 & -1 \\ w_{22} + \frac{w_{23}}{r_A} & -1 & 0 \\ w_{32} + \frac{w_{33}}{r_A} & \frac{1}{r_B} & 0 \end{pmatrix} \begin{pmatrix} \Delta\mu_A \\ \Delta\mu_B \\ \mu_B \end{pmatrix} = - \begin{pmatrix} J \cdot w_{14} \\ J \cdot w_{24} \\ J \cdot w_{34} \end{pmatrix} \quad (3.7)$$

where w_{ij} are the elements of the transfer matrix of the entire system (i.e. \mathbf{W}).

3.3 Calculate boundary values

The third step consists of calculating the boundary values (BVs) of the system, i.e. the state vectors between all the layers and interfaces \mathbf{x}_i with $i \in [1, 2N + 2]$. This is done by first solving the linear system (3.7) using an analytical solution from Mathematica which yields a numerical value for $\Delta\mu_A$. This, combined with 3.4 and 3.5c and the fact that J is known, allows us to calculate \mathbf{x}_A :

$$\mathbf{x}_A = \begin{pmatrix} \mu_A \\ \Delta\mu_A \\ \Delta J_A \\ J_A \end{pmatrix} = \begin{pmatrix} 0 \\ \Delta\mu_A \\ \Delta\mu_A/r_A \\ J \end{pmatrix}. \quad (3.8)$$

Once \mathbf{x}_A is known, the rest of the BVs are calculated by propagation through the layers and interfaces, using their corresponding transfer matrices (2.10).

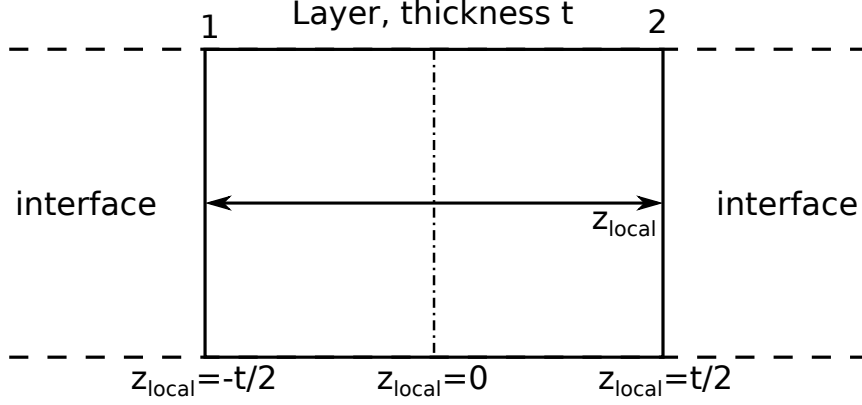


Figure 3.1: Definition of a local coordinate system for a layer.

3.4 Calculate integration constants

After the BVs are calculated, the solver performs the fourth and last step. This step consists of calculating the integration constants from the BVs and with that obtaining the full spatial solution of the system. As can be seen in 2.9, the general solutions to the system contain three integration constants. The first of these is $K_1^{(n)}$. Before calculating $K_1^{(n)}$, we first define local coordinate systems for the layers like in figure 3.1.

Now that we have our system of reference, we continue by deriving $K_{1,2,3}^{(n)}$ such that the local solutions in the layer match with the earlier obtained BVs. Since $K_1^{(n)}$ is the only unknown in $\mu^{(n)}(z)$ (2.9a), simply substituting $z = -\frac{t_n}{2}$ and $\mu^{(n)}(-\frac{t_n}{2}) = \mu_1^{(n)}$ (i.e. the BV on the left side of the layer) gives us an expression which can be solved easily for $K_1^{(n)}$:

$$\boxed{K_1^{(n)} = \mu_1^{(n)} + \frac{1}{2}\alpha_n t J - \beta_n \Delta\mu_1^{(n)}}. \quad (3.9)$$

Calculating $K_2^{(n)}$ and $K_3^{(n)}$ is slightly more complicated, since they both appear in the expression for $\Delta\mu^{(n)}(z)$ (2.9b). Two unknowns means we need two expressions: one is obtained by substituting $z = -\frac{t_n}{2}$ and $\Delta\mu^{(n)}(-\frac{t_n}{2}) = \Delta\mu_1^{(n)}$ and one by substituting $z = +\frac{t_n}{2}$ and $\Delta\mu^{(n)}(+\frac{t_n}{2}) = \Delta\mu_2^{(n)}$ into 2.9b. Solving this system of equations yields the expressions for $K_2^{(n)}$ and $K_3^{(n)}$:

$$\boxed{K_2^{(n)} = \frac{1}{\sinh \delta_n} \left[\Delta\mu_2^{(n)} e^{\delta_n/2} - \Delta\mu_1^{(n)} e^{-\delta_n/2} \right]}, \quad (3.10a)$$

$$\boxed{K_3^{(n)} = \frac{1}{\sinh \delta_n} \left[\Delta\mu_1^{(n)} e^{\delta_n/2} - \Delta\mu_2^{(n)} e^{-\delta_n/2} \right]}. \quad (3.10b)$$

Now we can simply substitute these integration constants into 2.9 to obtain the final solutions for μ , $\Delta\mu$ and ΔJ inside the layers.

3.5 Precision

One major issue that occurred with this transfer matrix method has to do with the precision at which the floating points are handled. When the solver steps, described in the sections above, were implemented correctly, the results showed incorrect behavior for a lot of system setups, mainly ones with relatively thick layers, or ones with a relatively high number of layers.

As can be seen in 3.11, the element $\mathbf{W}_{\text{layer},14}^{\text{VF}}$ consists of two parts: one linear in δ and one hyperbolic in δ , i.e. $\mathbf{W}_{\text{layer},14}^{\text{VF}} = A \cdot \delta + B \sinh \delta$. Upon investigation, it turned out that the failure of the solver occurred when the relative difference between these linear and hyperbolic terms became of 19 orders of magnitude, i.e. $\sinh \delta / \delta \sim 10^{19}$

$$\mathbf{W}_{\text{layer}}^{\text{VF}} = \begin{pmatrix} 1 & \beta (\cosh \delta - 1) & \beta r \sinh \delta & (1 - \beta^2)r_{\text{sf}}\delta + \beta^2 r_{\text{sf}} \sinh \delta \\ 0 & \cosh \delta & r_{\text{sf}} \sinh \delta & \beta r_{\text{sf}} \sinh \delta \\ 0 & \frac{1}{r_{\text{sf}}} \sinh \delta & \cosh \delta & \beta (\cosh \delta - 1) \\ 0 & 0 & 0 & 1 \end{pmatrix}. \quad (3.11)$$

At this point, a 80-bit container with a 63-bit mantissa ¹ was used to store floating point variables. Calculating the precision of the datatype yields:

$$2^{63} = 9.223372036854776 \cdot 10^{18} \approx 10^{19} \quad (3.12)$$

or a precision of 19 orders of magnitude. This coincidence led to the hypothesis, that the loss of the linear term in $\mathbf{W}_{\text{layer},14}^{\text{VF}}$ due to a lack of precision led to the failure of the solver.

In order to increase the precision and thereby solve this issue, an arbitrary precision container for floats, following the IEEE 754-2008 standard, was implemented. This container allows all bitwidths which are a multiple of 32.

After implementing this arbitrary precision model and increasing the bitwidth, the output of the solver turned out to be physically correct (see chapter 4). All the results in chapter 4 were obtained using a bitwidth of 1856.

¹The mantissa is the part of the container used to store the actual number. The rest is used for the sign and the exponent.

Chapter 4

Results

Now that it is clear what the solver calculates and with which methods, we can take a look at the results the solver produces. What the solver basically does is it calculates μ , $\Delta\mu$ and ΔJ for the given system, returns these calculated values and, if asked for, produces plots of these values throughout the system.

4.1 Identity Interface Model

4.1.1 NFN

First, the solver was tested on different systems using the identity matrix for all the interface transfer matrices. One of these systems is an NFN geometry (a ferromagnetic layer, sandwiched between two nonmagnetic layers) and its solutions can be seen in figure 4.1. Please note that a vector notation was used here to denote layer numbers (i.e. $\boldsymbol{\beta} = (\beta_1, \beta_2, \beta_3)$). Also, ρ^* and l_{sf} in the leads need to be known for the calculation of r_{sf} in the leads (3.5c and 3.6c). They are defined to be equal to ρ^* and l_{sf} in the adjacent N layers. The layers are separated by vertical, dotted lines. The solid lines represent the solution curves, the triangles the BVs.

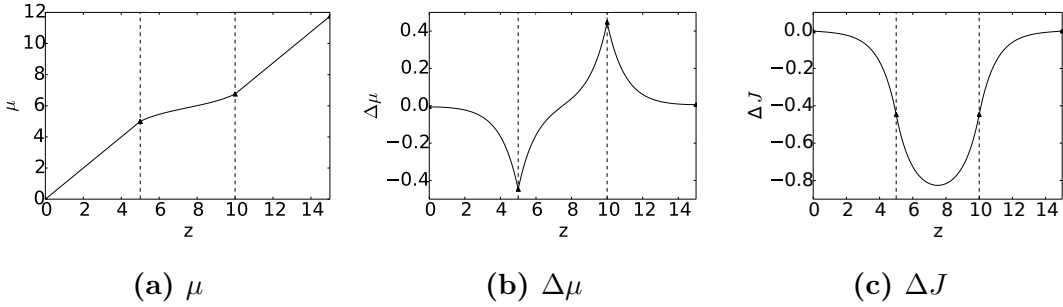


Figure 4.1: Solver results for an NFN geometry with $\mathbf{t} = (5, 5, 5)$, $\boldsymbol{\beta} = (0, 0.9, 0)$, $\boldsymbol{\rho}^* = (1, 1, 1)$, $\mathbf{l}_{\text{sf}} = (1, 1, 1)$ and $J = 1$.

Looking at figure 4.1, we see first of all that the solution curves match the BVs at the boundaries and that $\mu(z = 0) = 0$, as defined in 3.4. It can also be seen, that the derivative of the chemical potential is always positive. This is correct, since μ is proportional to V , with proportionality constant $e < 0$, and the voltage in a passive system in steady state never spontaneously rises. Also note the fact that the curve for μ is a straight line in the N layers, which is correct since J and ρ^* are constant within the layers. Further note the lack of discontinuities at the interfaces, which should be the case when using the identity interface model.

Furthermore, we can see that our system is symmetric around the center of the F layer ($z_{\text{local}} = 0$). We take this point as the origin of our global frame of reference. If we now do a thought experiment in which we reverse the direction of the total current density (i.e. $J_{\text{new}} = -J_{\text{old}}$), we can imagine that the behaviour of the system would remain exactly the same (since the system is symmetric), except for the reversed current direction. Mathematically, this means we can write the spin-dependent chemical potential and current density as functions of the global position z and J :

$$\mu^{\pm}(z, J) = \mu^{\pm}(-z, -J), \quad (4.1a)$$

$$J^{\pm}(z, J) = -J^{\pm}(-z, -J). \quad (4.1b)$$

If we now imagine sending in both the positive and the negative current, the total current density would become zero and the solutions for μ^{\pm} and J^{\pm} would be superpositions of the solutions for both currents. Since the total current would become zero, the solutions for $\mu^+(z)$ and $\mu^-(z)$ would be equal and constant:

$$\mu^{\pm}(z, J) + \mu^{\pm}(z, -J) = \text{const.} \equiv \alpha, \quad (4.2a)$$

$$\Rightarrow \boxed{\mu^{\pm}(z, J) = \alpha - \mu^{\pm}(-z, J)}, \quad (4.2b)$$

$$\text{with } \alpha = 2 \cdot \mu^{\pm}(0, J) \Rightarrow \mu^+(0) = \mu^-(0). \quad (4.2c)$$

$$J^{\pm}(z, J) + J^{\pm}(z, -J) = J^{\pm}(z, J) - J^{\pm}(-z, J) = 0, \quad (4.2d)$$

$$\Rightarrow \boxed{J(z, J) = J(-z, J)}. \quad (4.2e)$$

With this, we can now prove the symmetries in μ , $\Delta\mu$ and ΔJ , using the same, constant J throughout the derivation:

$$\mu(z) \equiv \frac{1}{2} \left(\mu(z)^+ + \mu(z)^- \right) \quad (4.3a)$$

$$\Rightarrow \mu(-z) = \frac{1}{2} \left(\mu(-z)^+ + \mu(-z)^- \right) = \frac{1}{2} \left(\alpha + \alpha - \mu(z)^+ - \mu(z)^- \right) \quad (4.3b)$$

$$\Rightarrow \mu(-z) = 2\mu(0) - \mu(z) \Rightarrow \underline{\text{antisymmetric with an offset.}} \quad (4.3c)$$

$$\Delta\mu(z) \equiv \frac{1}{2}(\mu(z)^+ - \mu(z)^-) \quad (4.3d)$$

$$\Rightarrow \Delta\mu(-z) = \frac{1}{2}(\mu(-z)^+ - \mu(-z)^-) = \frac{1}{2}(\alpha - \alpha - \mu(z)^+ + \mu(z)^-) \quad (4.3e)$$

$$\Rightarrow \Delta\mu(-z) = -\Delta\mu(z) \Rightarrow \underline{\text{antisymmetric.}} \quad (4.3f)$$

$$\Delta J(z) \equiv J(z)^+ - J(z)^- \quad (4.3g)$$

$$\Rightarrow \Delta J(-z) = J(-z)^+ - J(-z)^- = J(z)^+ - J(z)^- \quad (4.3h)$$

$$\Rightarrow \Delta J(-z) = \Delta J(z) \Rightarrow \underline{\text{symmetric.}} \quad (4.3i)$$

A similar derivation can be used to show that in an antisymmetrical geometry, $\mu(z)$ should be antisymmetric with an offset, $\Delta\mu(z)$ symmetric and $\Delta J(z)$ antisymmetric. As can be seen in figures 4.1 and 4.2, the predicted symmetries are present in the solver result.

Lastly, note that both $\Delta\mu$ and ΔJ have an exponential form in the nonmagnetic layers and go to zero as we go away from the F-N interface. This is correct since the N layers have the same properties (ρ^* , l_{sf} , β) as the leads, and inside the leads any deviations from equilibrium should decay exponentially, since the system is governed by a spin-diffusion type equation (2.5).

4.1.2 Spin Valves

In addition to the NFN system, the solver was also tested on the parallel (P) and antiparallel (AP) spin valves, which are NFNFN geometries where the magnetizations in the F layers point respectively in equal and opposite directions.

The results of these spin valves can be seen in figure 4.2. Here it can be seen that all the signs of correctness that were checked with the NFN geometry also hold for the two spin valves. Note that for the AP spin valve the magnetization is antisymmetric in z around the center of the geometry, whereas for the P spin valve it is symmetric. This can be seen in figure 4.2 by the fact that $\Delta\mu$ has an antisymmetric solution and ΔJ a symmetric one in the P case, while $\Delta\mu$ has a symmetric solution and ΔJ an antisymmetric one in the AP case.

The idea of a spin valve is that only one of the F layers is susceptible to external magnetic fields. If the direction of the to-be-measured magnetic field is known beforehand, the spin valve can be constructed in such a way, that a lack of a (sufficiently strong) field yields a P state, while the to-be detected field would yield an AP state. This state difference can then be detected through the effect that an AP spin valve has a different electrical resistance compared to a P valve. This effect is called giant magnetoresistance (GMR) and can be seen in figure 4.3: in this figure, the solutions to a P (black) and an AP (red) spin valve are plotted in the same graphs. In figure 4.6a it can be seen that the AP state indeed yields a larger increase in the chemical potential and therefore a larger potential drop than the P state.

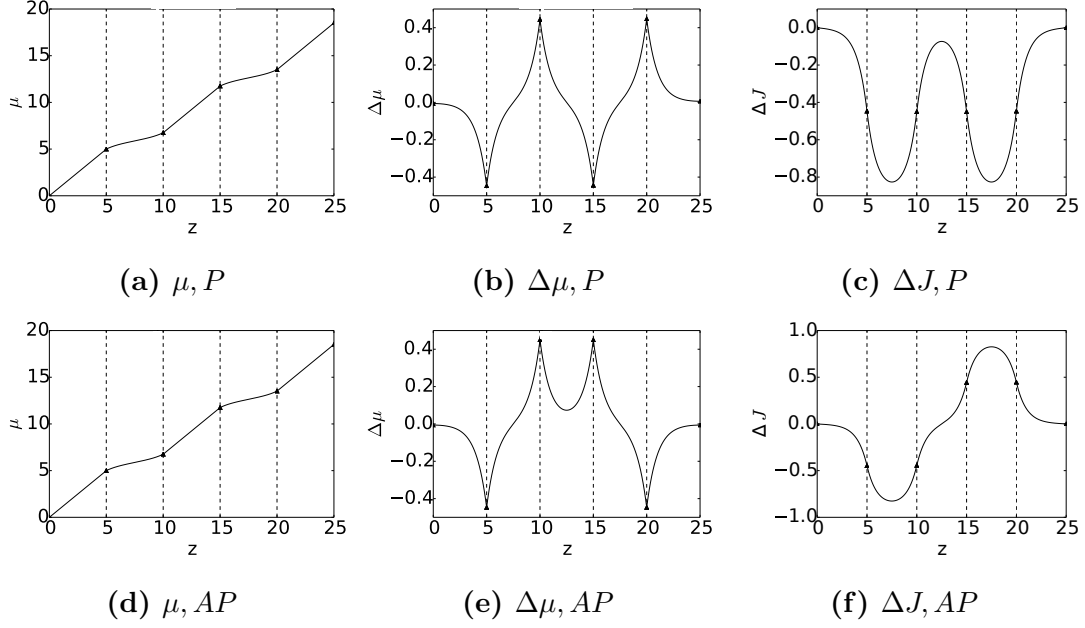


Figure 4.2: Solver results for the P and AP spin valve geometries with $\mathbf{t} = (5, 5, 5, 5, 5)$, $\boldsymbol{\beta}^\pm = (0, 0.9, 0, \pm 0.9, 0)$, $\boldsymbol{\rho}^* = (1, 1, 1, 1, 1)$, $\mathbf{l}_{\text{sf}} = (1, 1, 1, 1, 1)$ and $J = 1$.

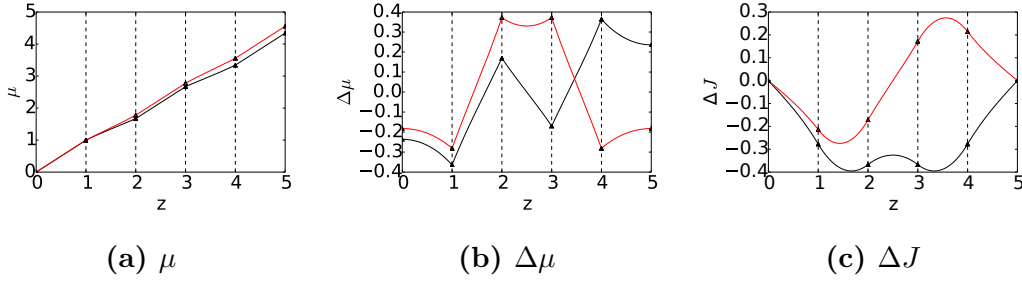


Figure 4.3: Solver results for the P and AP spin valve geometries to show the effect of GMR. $\mathbf{t} = (1, 1, 1, 1, 1)$, $\boldsymbol{\beta}^\pm = (0, 0.9, 0, \pm 0.9, 0)$, $\boldsymbol{\rho}^* = (1, 1, 1, 1, 1)$, $\mathbf{l}_{\text{sf}} = (1, 1, 1, 1, 1)$ and $J = 1$.

4.2 Non-identity Interface Models

After this, the solver was tested on the NFN geometry, using different interface models. All the following results, including this section and the next one, are obtained using the following parameters: $\mathbf{t}=(1,1,1)$, $\boldsymbol{\beta} = (0, 0.9, 0)$, $\boldsymbol{\rho}^* = (1, 1, 1, 1, 1)$, $\mathbf{l}_{\text{sf}} = (1, 1, 1, 1, 1)$ and $J = 1$.

The first interface model is the Valet-Fert (VF) interface model and the results can be seen in figure 4.4. These results show the same signs of correctness as in figure 4.1: $\mu(0) = 0$, $\frac{\partial\mu}{\partial z} > 0$, curves that match the BVs, $\Delta\mu(\pm\infty) = 0$, $\Delta J(\pm\infty) = 0$, similar forms and (anti)symmetry. However, this time there is a step in μ and $\Delta\mu$ at the interfaces. On the contrary, ΔJ is still continuous, albeit non-smooth. Looking back at figure 2.2, we see that these results are in line with the theory,

since in a series circuit the voltage can drop but the current will be conserved. The fact that there is a step in $\Delta\mu$, even though $R_A = R_B$, can be explained with the fact that the incident ΔJ is not zero, as can be seen in figure 4.4c. Since $\mu_2^\pm - \mu_1^\pm = R \cdot J_{1,2}^\pm$, the drops in μ^+ and μ^- are not equal and thus there is a step in $\Delta\mu$ at the interface.

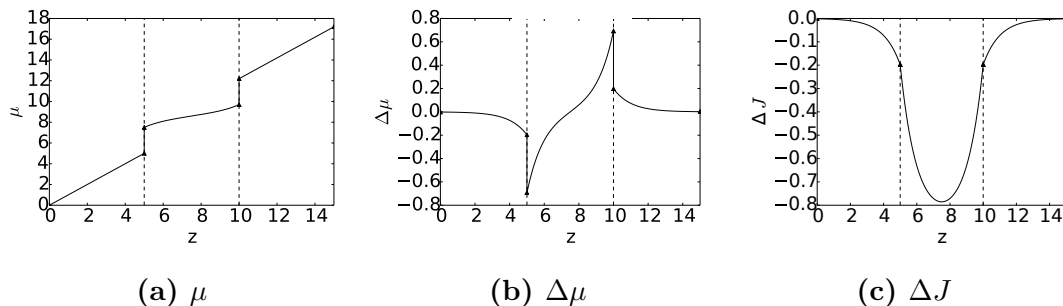


Figure 4.4: Solver results for the NFN geometries. $\text{im}=\text{VF}$, $R_A = 5$, $R_B = 5$.

The results for the Bass-Pratt (BP) and 6 resistance (R6) interface models can be found respectively in figures 4.5 and 4.6. Again, the same signs of correctness can be seen as in the previous figures. Apart from that, we can see that this time there are steps at the interfaces in all the variables.

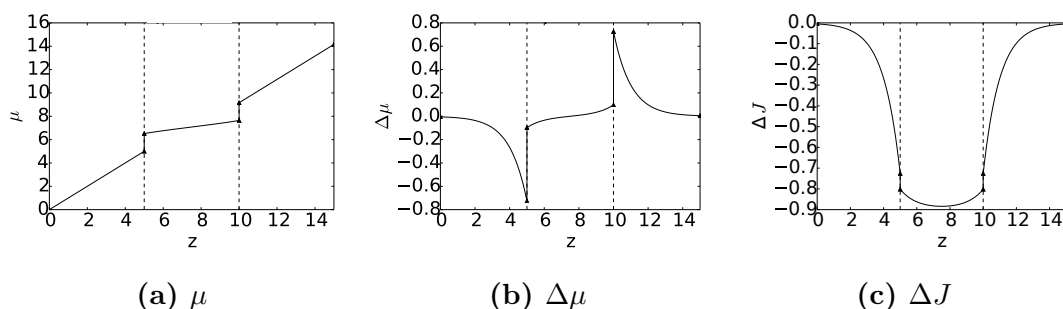


Figure 4.5: Solver results for the NFN geometries. $\text{im}=\text{BP}$, $\gamma = 0.9$, $\delta_{\text{int}} = 1$, $r_{\text{int}} = 5$.

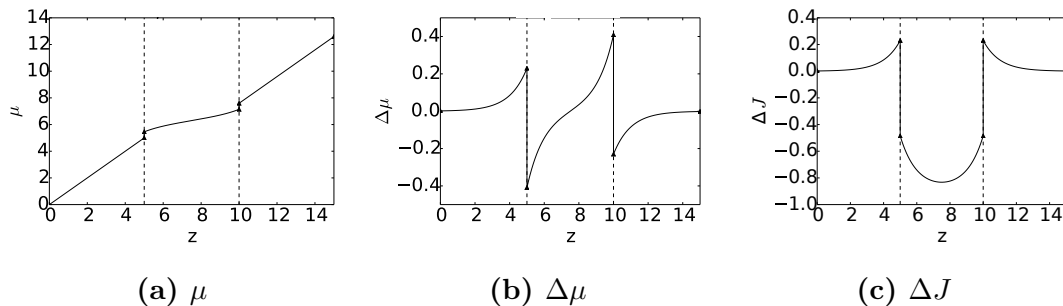


Figure 4.6: Solver results for the NFN geometries. $\text{im}=\text{R6}$, $R_A = 0.1, R_B = 0.1, R_C = 1, R_D = 1, R_E = 1, R_F = 1$.

4.3 Interface Parameter Dependent Step Sizes

So when using a non-identity interface model, we get steps in $\mu, \Delta\mu, \Delta J$ at the interfaces. This fact, however, is not a very interesting result. What is more interesting is how those interface step sizes depend on the interface model parameters. In order to study these dependencies, we define $\Delta\mu_{\text{avg.}}$ and $\Delta\mu_{\text{step}}$ according to 4.4.

$$\Delta\mu_4 \equiv \Delta\mu_{\text{avg.}} + \Delta\mu_{\text{step}}, \quad (4.4a)$$

$$\Delta\mu_3 \equiv \Delta\mu_{\text{avg.}} - \Delta\mu_{\text{step}}. \quad (4.4b)$$

We conduct similar definitions for $\mu_{\text{avg.}}, \mu_{\text{step}}, \Delta J_{\text{avg.}}$ and ΔJ_{step} . The values for the NF interface, containing the 3rd and 4th BVs (see figure 2.1), were used.

4.3.1 Valet-Fert

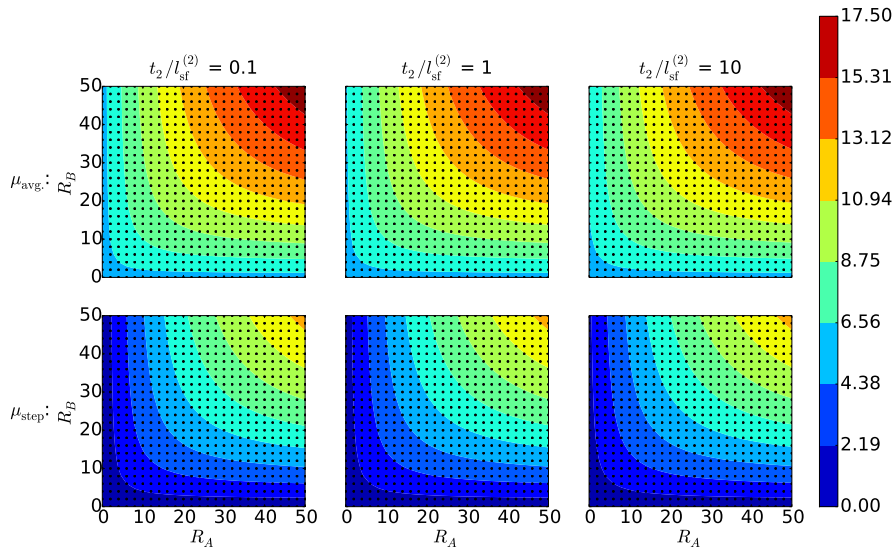
The parameter space of the Valet-Fert interface model (VFIM) spans only two dimensions: R_A and R_B . However, since we are also interested in the effects of spin accumulation, the layer thickness over the spin-diffusion length of the F layer (i.e. $t_2/l_{\text{sf}}^{(2)}$) was added as a third dimension. In plot sheets, we are able to visualize four dimensions: two on the plots axes and two on the plot grid on the sheet. The fourth and last dimension was used to portray either the values for both spins or the values for both the step and the average in the same plot (see figure 4.7).

Looking at figure 4.7a, that μ_{step} goes to zero as R_A and R_B go to zero. This is correct, since two parallel, resistanceless channels let the incoming signal pass through unchanged. Also note that as R_A and R_B increase, μ_{step} and $\mu_{\text{avg.}}$ seem to evolve as $[R_A^{-1} + R_B^{-1}]^{-1}$. This is correct, since that is the formula for the total resistance of two parallel resistances.

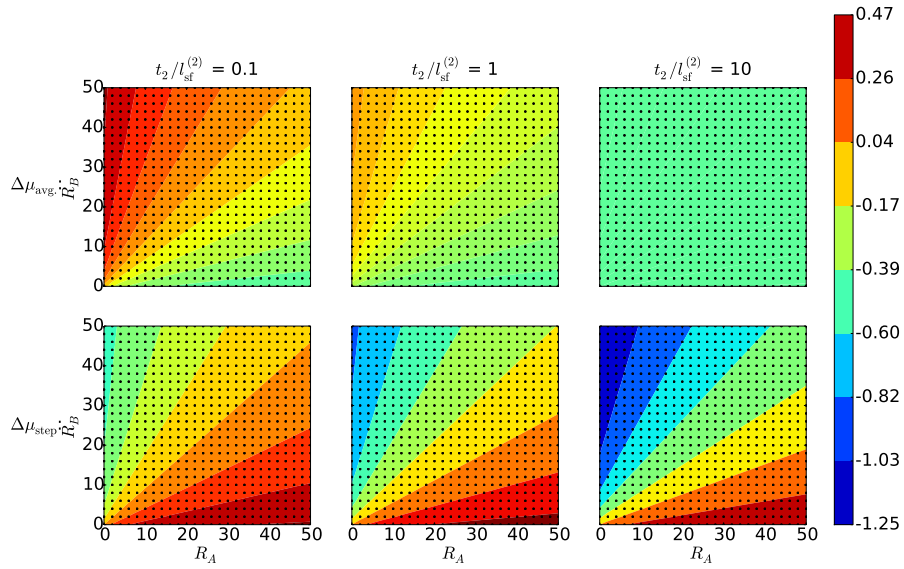
Looking at figure 4.7b, we see that $\Delta\mu_{\text{step}}$ increases as R_A increases. This seems correct, since if R_A increases we expect $(\mu_4^+ - \mu_4^-)$ to increase, meaning that $\Delta\mu_{\text{step}}$ increases. The opposite holds for R_B and $\Delta\mu_{\text{step}}$. Also note that when R_A and R_B are equal, $\Delta\mu_{\text{step}}$ does not become zero. This is due to the fact that the spin-up current encounters more resistance in the F layer than the spin-down current (i.e. $\rho_{\uparrow} < \rho_{\downarrow}$), meaning that $J^+ \neq J^-$ when $R_A = R_B$, causing a difference in the two spin-dependent chemical potential steps.

Furthermore, when we compare 4.7b to 4.7c, we see that

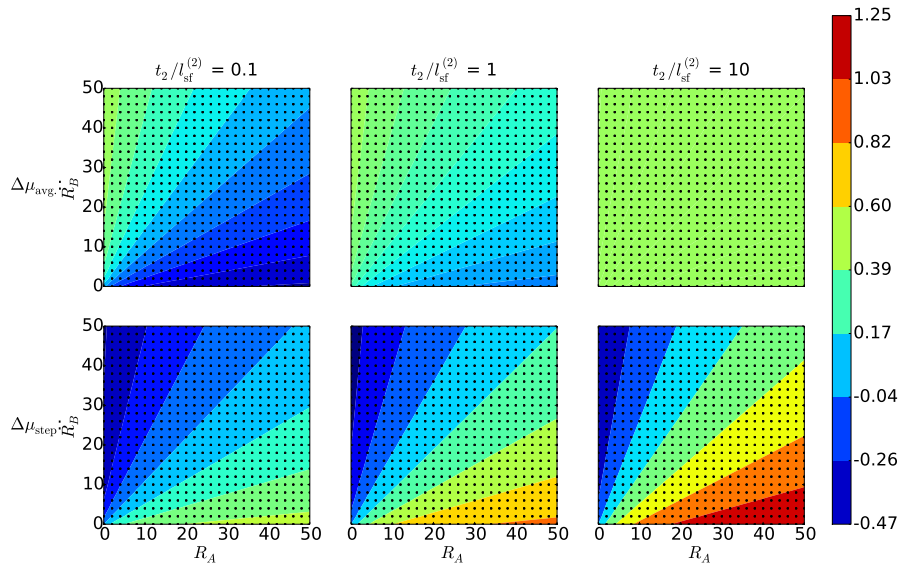
$\Delta\mu_{\text{step}}(\beta_2 = 0.9) > \Delta\mu_{\text{step}}(\beta_2 = -0.9)$. This effect seems logical if we think of the NF interface and the F layer as two parallel series circuits, neglecting spin-flipping (which is a relatively small effect anyways). If $\beta_2 = 0.9 \Rightarrow \rho_{\uparrow} < \rho_{\downarrow}$ in the F layer, causing $(\mu_4^+ - \mu_4^-)$ to increase and $(\mu_3^+ - \mu_3^-)$ to decrease and thus $\Delta\mu_{\text{step}}(\beta_2 = 0.9)$ to increase. Since the opposite is true for $\beta_2 = -0.9$, $\Delta\mu_{\text{step}}(\beta_2 = 0.9) > \Delta\mu_{\text{step}}(\beta_2 = -0.9)$ seems correct.



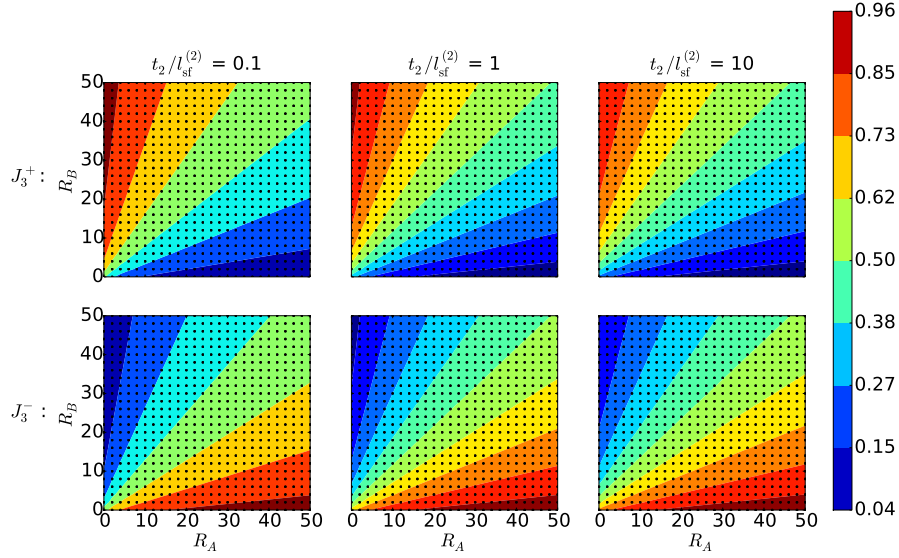
(a) μ_{step} and μ_{avg} . for $\beta_2 = +0.9$



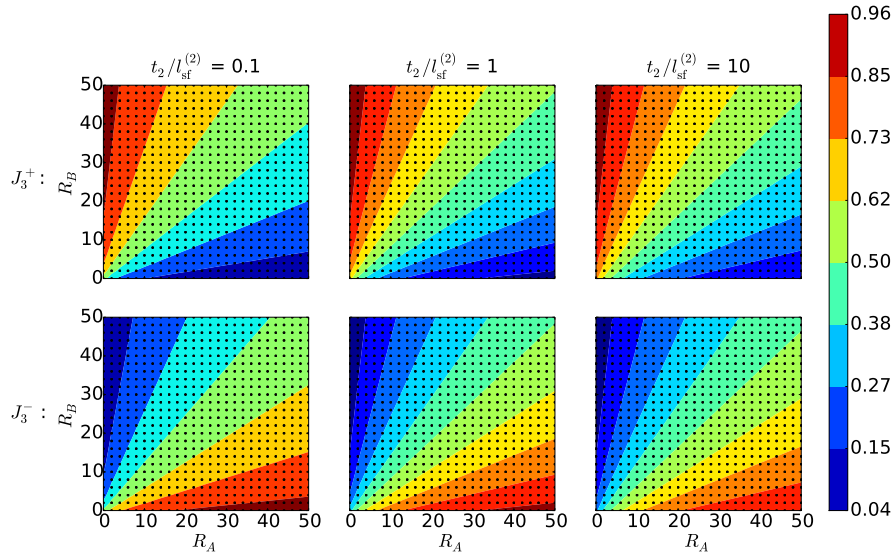
(b) $\Delta\mu_{\text{step}}$ and $\Delta\mu_{\text{avg}}$. for $\beta_2 = +0.9$



(c) $\Delta\mu_{\text{step}}$ and $\Delta\mu_{\text{avg}}$. for $\beta_2 = -0.9$



(d) J^+ and J^- for $\beta_2 = +0.9$



(e) J^+ and J^- for $\beta_2 = -0.9$

Figure 4.7: Step sizes in and average interface values of μ , $\Delta\mu$ and J^+ , J^- plotted vs. R_A , R_B and $t_2/l_{\text{sf}}^{(2)}$ for $\beta_2 \in (-0.9, 0.9)$ for the VFIM. Every dot represents the result of one simulation.

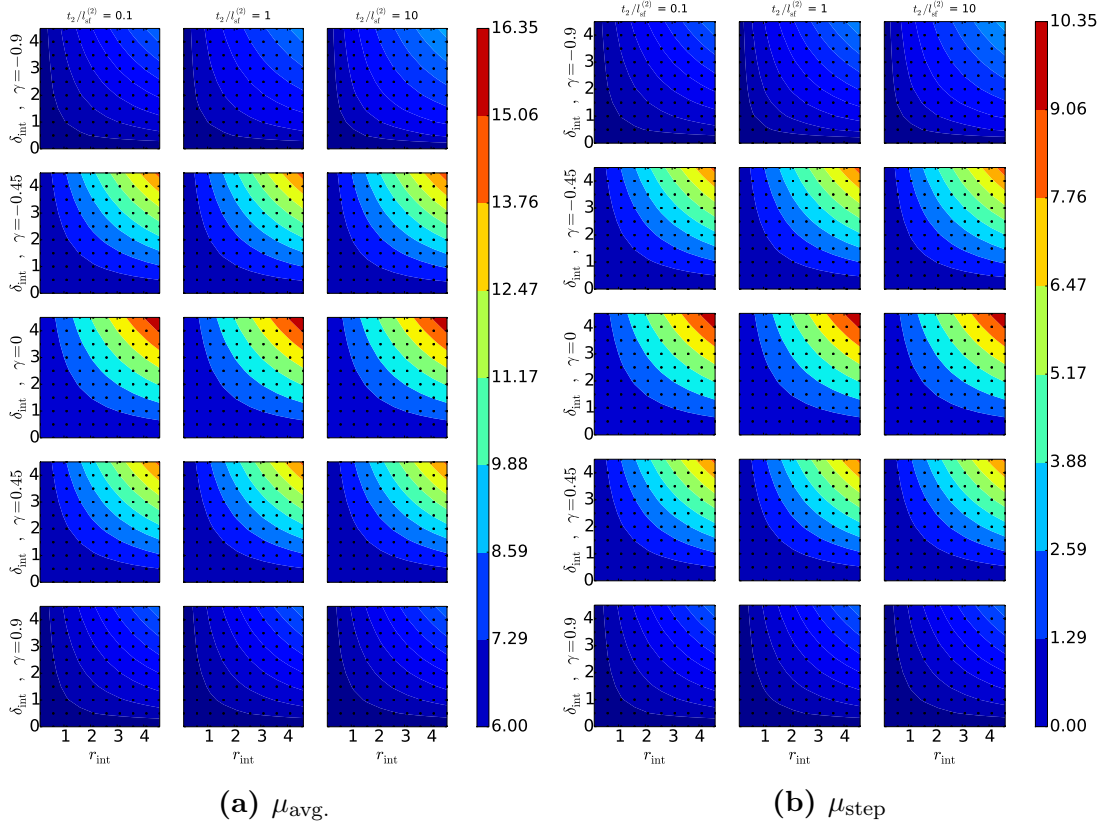


Figure 4.8: Step sizes in and average interface values of μ plotted vs. γ, r, δ and $t_2/l_{\text{sf}}^{(2)}$ for $\beta_2 = 0.9$ for the BPIM. Every dot represents the result of one simulation.

If we look at figures 4.7d and 4.7e, we see that an increase in R_A leads to an decrease in J^+ and an increase in J^- and that the opposite hold for an increase in R_B . This is correct, since the current drops as the resistance increases and $J = J^+ + J^- = \text{const.}$

Finally, increasing $t_2/l_{\text{sf}}^{(2)}$ basically represses the effects caused by the difference in ρ_{\uparrow} and ρ_{\downarrow} . This can be seen in figures 4.7d and 4.7e, where for $\beta_2 = 0.9$, J^+ decreases and J^- increases, while $\rho_{\uparrow} < \rho_{\downarrow}$. For $\beta_2 = -0.9$, J^+ increases and J^- decreases, while $\rho_{\downarrow} < \rho_{\uparrow}$.

4.3.2 Bass-Pratt

The parameter space of the Bass-Pratt interface model (BPIM) spans three dimensions: γ, r_{int} and δ_{int} , equivalent to β, r_{sf} and δ for the VF layer transfer matrix. Since we are again also interested in the effects of spin accumulation, the layer thickness over the spin-diffusion length of the F layer (i.e. $t_2/l_{\text{sf}}^{(2)}$) was added as a fourth dimension. In plot sheets, we are able to visualize four dimensions: two on the plots axes and two on the plot grid on the sheet. (see figures 4.8 and 4.9). Looking at figure 4.8b, we see that as γ increases μ_{step} decreases, which was to be

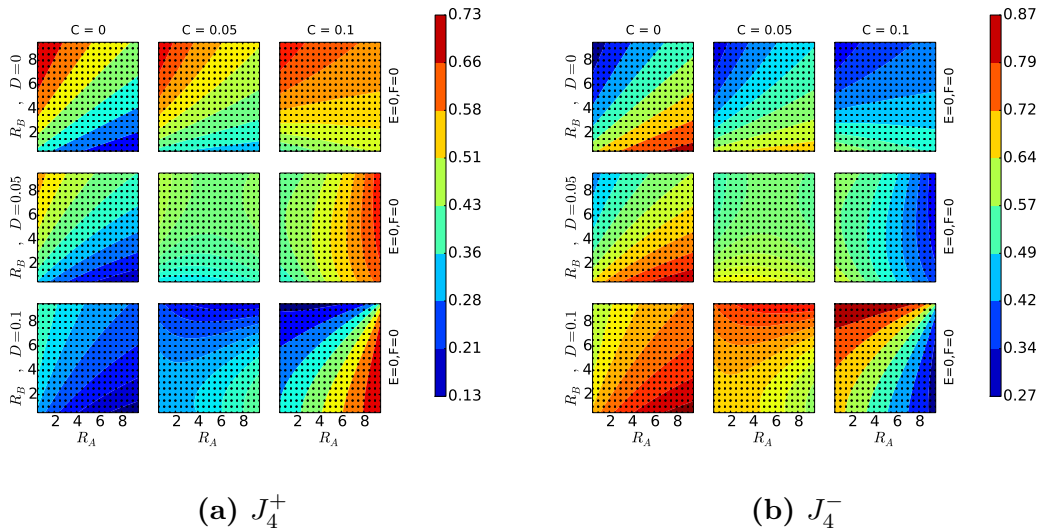


Figure 4.10: J_4^+ and J_4^- plotted vs. R_A, R_B, C, D for $t_2/l_{\text{sf}}^{(2)} = 1$, $\beta_2 = 0.9$ and $E, F = 0$ for the R6IM. Every dot represents the result of one simulation.

expected since the virtual layer resistance $r = r_{\text{sf}}\delta(1 - \gamma^2)$. Also since the BPIM uses a virtual layer to describe an interface one would expect to see some coupling between γ and β_2 , just the coupling that the principle of GMR is based upon. As can be seen in the plots by comparing the result for $\gamma = 0.9$ and $\gamma = -0.9$ or $\gamma = 0.45$ and $\gamma = -0.45$, when γ is positive (i.e. aligned with β_2) the step in μ is slightly smaller, but the effect is very minimal.

By looking at the figure, we can see that the plots confirm that $\mathbf{W}_{\text{int}}^{\text{BP}}$ is equal to the identity matrix for $\delta_{\text{int}} = 0$, which is correct, since a layer with thickness zero can not have any effects. We could continue this kind of explanation for all the effects of the BPIM and pointing out that they are indeed equivalent to the effects an actual F or N layer. However, the most important point to notice when examining the BPIM is that its behaviour is more complicated (see figures 4.9a and 4.9b) and less directly correlated to its parameters in comparison to the VFIM and (as will become clear in the next subsection) the 6 resistances model.

4.3.3 6 Resistances

The parameter space of the 6 resistances interface model (R6IM) spans six dimensions: A,B,C,D,E and F. Since the reciprocals of A and B ($A^{-1} = R_A, B^{-1} = R_B$) are equivalent to R_A and R_B in the VFIM, R_A and R_B were varied on the x- and y-axis respectively, just as was done for the VFIM. This way, the plots of the R6IM can be compared easily to those of the VFIM. When we compare figures 4.10b and 4.10b to 4.7d, we see first of all that the results for the R6IM for conductances C,D,E,F=0 are equivalent to the result obtained from the VFIM. This is correct, since when we equate the conductances C,D,E,F to zero (i.e. remove those connections from the R6IM), we are simply left with the VFIM.

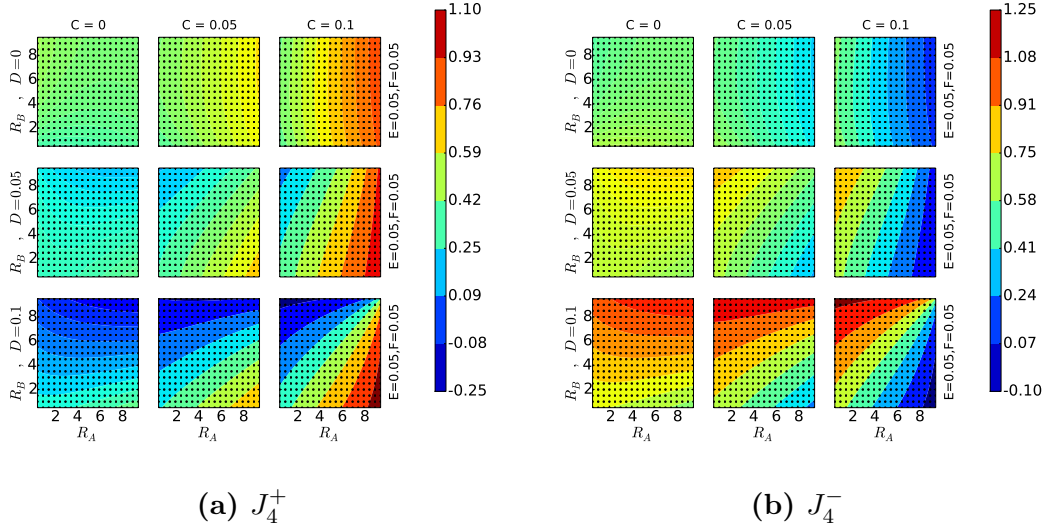


Figure 4.11: J_4^+ and J_4^- plotted vs. R_A, R_B, C, D for $t_2/l_{\text{sf}}^{(2)} = 1$, $\beta_2 = 0.9$ and $E, F = 0.05$ for the R6IM. Every dot represents the result of one simulation.

Furthermore, by looking at the figure, we see that J_4^+ increases and J_4^- decreases as we increase C . This inverse is the case as we increases D . This is in agreement with the expected behaviour from the electrical circuit (see figure 2.3). However, we can also see in the figure that J_4^+ and J_4^- show similar behaviour when we increase both C and as when $C, D=0$, but mirrored around the line $R_A = R_B$. Why this is, is not entirely clear.

Finally, by comparing figures 4.11a and 4.11b to 4.10a and 4.10b we see that increases E and F decreases the differences between the two spin currents. This is correct, since increasing the conductivity of E and F , both the spin accumulation on the left side (i.e. the difference between μ_3^+ and μ_3^-) and on the right side (i.e. the difference between μ_4^+ and μ_4^-) of the interface are allowed to relax out more. When we also increase C , it can be seen in the figure that J_4^+ and J_4^- become less dependent on R_A . The same is the case for increased D and less dependence on R_B .

Chapter 5

Conclusions

First of all, we can conclude that the solver created for this report allows for the correct calculation of spin transport through magnetic multilayers according to the theory from the VF paper, when using the identity interface model. The other interface models seem to be implemented correctly as well, since the results seem to behave as expected.

As for the behaviour of the the three interface models, the Valet-Fert interface model proved to be a simple and relatively easy to understand interface model. However, as was known beforehand, it is not able to model spin-flipping at the interfaces.

The Bass-Pratt interface model is able to model more complicated behaviour. Also, since it behaves just as a (ferro)magnetic layer, we can simply apply all acquired knowledge of the VF theory of spin transport to predict the behaviour of this interface model. However, since it models more complicated behaviour with only three parameters, its behaviour seems to be less directly correlated to its parameters, which might make it harder to match the interface model to actual (theoretically of experimentally determined) behaviour at an interface.

The 6 resistances interface model is able to model a relatively large amount of interface transport behaviours (interface reflection and transmission, spin-flipping and spin-conserving). Also, the way individual parameters affect the behaviour of the interface model are relatively easy to predict by simply applying Ohm's law. However, since it uses a quite complicated electrical circuit to model the behaviour, the model itself would need an in-depth analysis to be understood fully.

Chapter 6

Future Recommendations

First of all, the solver created for this report is still in a very user-unfriendly state. Some pieces of interface codes were written in order to be able to call the solver back-end more easily, to be able to change the solver input without having to write them into the solver code itself and to be able to comfortably perform parameter sweeps with the solver to create plot sheets like the one in figure 4.7. However, most tasks still require the user to edit the back-end, which is not practical for anyone who has not written the code itself.

Therefore, the first recommendation would be to improve the interface codes to the point where one could use the solver without ever having to touch the back-end.

Furthermore, all the plot sheets that can be seen in this report were created using simulations on NFN geometries. In order to gain a deeper understanding of the behaviour of the interface models, plot sheets would have to be created and analyzed using different geometries (e.g. spin valves).

Also, most results in this report are about the properties of the different interface models and the dependencies of their behaviour on their parameters. Some comments on the differences between the models were made, but a final conclusion on the limits of the models and on what model is capable of modelling what is not reached. Therefore, further analysis on the limits of the different interface models is recommended.

References

- [1] T. Valet and A. Fert, PRB 48 (1993) 7099
- [2] R.J.H. Wesselink, PhD. thesis, unpublished
- [3] W. P. Pratt and J. Bass, JMMM 200 (1999) 274-289